EFFECTS OF AEROSOL SCATTERED RADIATION ON MINOR ATMOSPHERIC SPECIES CONCENTRATIONS IN A ONE-DIMENSIONAL MODEL

Hideaki YAMAMURA, Motokazu HIRONO,

Department of Physics, Faculty of Science, Kyushu University, Hakozaki, Higashi-ku, Fukuoka 812

Osamu UCHINO and Mitsuo MAEDA

Department of Electrical Engineering, Faculty of Engineering, Kyushu University, Hakozaki, Higashi-ku, Fukuoka 812

Abstract: The effects of solar radiation scattered by aerosols on minor atmospheric species concentrations were examined by a one-dimensional transport-kinetics model with radiative transfer model including the effects of absorption and multiple scattering by molecules and aerosols. The absorption and scattering of aerosols significantly affect the photodissociation rates of optically active species and lead to changes in the concentration profiles of atmospheric minor constituents. For example, a few percent decrease in the stratospheric ozone concentration is simulated for the increased aerosols. The sensitivity of the ozone concentrations to changes in the aerosol loads was also examined.

1. Introduction

Atmospheric aerosols have significant effects on the radiation fields in the atmosphere. For example, if an intense aerosol layer is assumed to exist at a height of about 20 km, the photodissociation rates of atmospheric molecules above 20 km will increase by partially reflected radiation into the outer space. The effects of absorption and multiple scattering by molecules and aerosols and of surface albedo on the direct and diffused solar radiation fields and the photodissociation rate of ozone (FIOCCO *et al.*, 1978) and other species (MUGNAI *et al.*, 1979) have been discussed. According to FIOCCO *et al.* (1978), an increase in the aerosol loads results in an enhancement in the photodissociation of ozone except near the ground.

Changes of molecular photolysis of species should affect the concentration profiles of atmospheric minor constituents. The effects of only molecular multiple scattering and surface albedo on atmospheric photodissociation rates have been discussed by LUTHER and GELINAS (1976), and PITARI and VISCONTI (1979). Enhanced photodissociation rates of many species were obtained when compared with those calculated in most of atmospheric photochemical models which only describe absorption in a direct solar beam. Using the enhanced photodissociation rates, LUTHER *et al.* (1978) calculated a one-dimensional transport-kinetics model and obtained dramatic changes in the concentration profiles of many trace species. They concluded

that it is important to include molecular multiple scattering and surface albedo when model results are compared with observational data.

In this paper the effects of absorption and multiple scattering by aerosols as well as molecules were investigated on various species concentrations by *coupling* a radiative transfer computation *with* a one-dimensional transport-kinetics model. The difference between the results of atmospheric species photodissociations calculated for a case of no aerosol loads and those for three cases of aerosol loads was examined. The effects of enhanced stratospheric aerosol layers after the violent volcanic eruptions of El Chichon on the ozone concentrations were also investigated.

2. Model Description

Calculation was performed in the following procedure.

1) Computation of a radiative transfer model: solar radiation fields in the atmosphere as a function of altitude and wavelength and the resultant photodissociation rates of optically active species are calculated. This radiative transfer computation accounts for the effects of absorption and scattering by aerosols and molecules, and for the ground albedo, and the solar zenith angle. The molecular absorption due to O_3 and O_2 is taken into account. The absorption and scattering by aerosols are determined by the Mie scattering theory. The spectral region of computation is 1810–7300Å.

2) Computation of a one-dimensional atmospheric transport-kinetics model: the concentration profiles of minor constituents are calculated using the photodissociation rates of molecules calculated in 1). Reaction of O_x, NO_x and HO_x is considered in the model.

3) The ozone concentration calculated by the one-dimensional atmospheric model is fed into 1) and the processes 1)–3) are repeated until the concentrations of constituents are in a steady state.

2.1. Radiative transfer model

To obtain the solar radiative flux in the atmosphere as a function of altitude, wavelength and solar zenith angle, computation of the radiative transfer model is carried out in the following procedure. The radiative transfer model considers the effects of absorption and scattering from molecules and aerosols and of the ground albedo, and assumes a cloudless, plane-parallel atmosphere and the azimuthally averaged radiation. The radiation fields can be divided into the solar direct beam and the specular reflected beam from the earth's surface, and the diffuse component due to the scattering and thermal emission from the atmosphere and the ground. Therefore, the total intensity I_{tot} is split with two components, the direct intensity I_{dir} and the diffuse intensity I_{dif},

$$I_{\mathrm{tot}}=I_{\mathrm{dir}}+I_{\mathrm{dif}}\,. \tag{1}$$

For the diffuse intensity, the monochromatic azimuthally integrated radiative transfer equation in the plane-parallel atmosphere can be written as follows,

$$\left(\mu\frac{\partial}{\partial\tau}+1\right)I(\tau,\mu)=\sigma(\tau,\mu)+\frac{\omega(\tau)}{2}\int_{-1}^{1}P(\tau,\mu,\mu')I(\tau,\mu')\mathrm{d}\mu'\,, \tag{2}$$

where $I(\tau, \mu)$ is the azimuthally averaged intensity in the direction $\mu=\cos\theta$, θ being the angle measured away from the nadir, at the level of optical thickness τ of the atmosphere above it. This optical thickness is due to the absorption and scattering by molecules and aerosols. Thus,

$$\tau=\tau_{\mathrm{R}}^{\mathrm{s}}+\tau_{\mathrm{R}}^{\mathrm{a}}+\tau_{\mathrm{M}}^{\mathrm{s}}+\tau_{\mathrm{M}}^{\mathrm{a}}\,, \tag{3}$$

where $\tau_{\mathrm{R}}^{\mathrm{s}}$ is the Rayleigh scattering optical thickness which is calculated by the relations of PENNDOLF (1957). The optical thickness due to gaseous absorption $\tau_{\mathrm{R}}^{\mathrm{a}}$ includes only the absorption of O_3 and O_2. $\tau_{\mathrm{M}}^{\mathrm{s}}$ and $\tau_{\mathrm{M}}^{\mathrm{a}}$ are the scattering and absorption optical thickness by aerosols which are calculated for a given wavelength, size-distribution and refractive index by the Mie scattering theory following the procedure of DEIRMENDJIAN (1969). $\omega(\tau)$ is the single scattering albedo, *i.e.* the ratio of the scattering coefficient to the extinction coefficient. $P(\tau, \mu, \mu')$ is the azimuthally averaged normalized scattering phase function; incident radiation in the direction μ' is scattered to the direction μ. The phase function includes the Rayleigh and Mie scattering which is obtained by the definition of DEIRMENDJIAN (1969). $\sigma(\tau, \mu)$ is the source term. Since we will assume no sources of the thermal emission and specular reflection, the source term is given only by the solar direct source,

$$\sigma(\tau, \mu)=\frac{\omega(\tau)F_{\mathrm{s}}}{4\pi}P(\tau, \mu, \mu_{\mathrm{s}})\exp(-\tau/\mu_{\mathrm{s}})\,, \tag{4}$$

where F_{s} is the solar flux at the top of the earth's atmosphere, and μ_{s} is cosine of the solar zenith angle χ.

To save the computer time, the radiative equation for the diffuse intensity fields is approximated into the two-stream form based on the two-point quadrature (MEADOR and WEAVER, 1980). The equation is represented by the identical forms of coupled differential equations: the radiative intensity is replaced by that integrated over hemispheres,

$$\frac{\mathrm{d}I^{\pm}(\tau)}{\mathrm{d}\tau}=-\frac{I^{\pm}(\tau)}{\mu_1}+\sigma^{\pm}(\tau)+\frac{\omega(\tau)}{2\mu_1}\{P^{+}(\tau)I^{\pm}(\tau)+P^{-}(\tau)I^{\mp}(\tau)\}\,, \tag{5}$$

where $I^{\pm}(\tau)$ is the downward (upward) flux, and μ_1 is the quadrature point. $\sigma^{\pm}(\tau)$ and $P^{\pm}(\tau)$ are calculated as follows:

$$\sigma^{\pm}(\tau)=\int_0^1\sigma(\tau, \pm\mu)\mathrm{d}\mu\,,$$

$$P^{\pm}(\tau)=\int_0^1 P(\tau, \pm\mu, \mu_1)\mathrm{d}\mu\,. \tag{6}$$

To solve eq. (5), we refer to the procedure of FIOCCO *et al.* (1978) which is based on the algorithm developed by GRANT and HUNT (1969) and WISCOMBE (1976a, b). The algorithm is performed for the case of two-point quadrature ($\pm\mu_1$). The transmissivity, reflectivity and internal source in each model layer are determined by the "doubling method". The diffuse intensity in the atmospheric radiation fields is calculated by the algorithm of GRANT and HUNT (1969).

The direct intensity (purely absorbed radiation intensity of solar direct flux)

with no specular reflection from the earth's surface is determined by

$$I_{\mathrm{dir}}(\tau)=\frac{F_{\mathrm{s}}}{2\pi}\exp\left(-\tau/\mu_{\mathrm{s}}\right). \tag{7}$$

The radiative flux is obtained from the intensity. The direct F_{dir} and diffuse F_{dif} components of flux are given by

$$\begin{aligned} F_{\mathrm{dir}}&=2\pi I_{\mathrm{dir}}\,,\\ F_{\mathrm{dif}}&=2\pi(I^{+}_{\mathrm{dif}}+I^{-}_{\mathrm{dif}})\,. \end{aligned} \tag{8}$$

The total flux F_{tot} is obtained from a sum of the direct and diffuse components, as follows,

$$F_{\mathrm{tot}}=F_{\mathrm{dir}}+F_{\mathrm{dif}}\,. \tag{9}$$

The photodissociation rate of ith species is given by the following expression:

$$J_i(\tau)=\int_{\Delta\lambda_i}\frac{\lambda}{hc}\sigma_i(\lambda)F(\tau,\,\lambda)\mathrm{d}\lambda\,, \tag{10}$$

where $\sigma_i(\lambda)$ is the absorption cross-section of ith species for the wavelengh λ. h and c are Planck's constant and the light velocity, respectively. $\Delta\lambda_i$ is the spectral region where photodissociation takes place (Table 1).

These procedures are valid only for the case of monochromatic radiation. We assume the radiation of a small wavelength interval $\delta\lambda$ to be monochromatic when the quantities such as the absorption and scattering properties of atmospheric components and the solar incident flux vary gradually and by small amount with wavelength over the small interval. Therefore, the spectral region $\Delta\lambda$ was divided by the small interval $\delta\lambda$ of unequal widths and the average values over the interval are calculated as the monochromatic procedures. The integral of the photodissociation coefficient over the spectral region is replaced by the sum of the average values in the intervals. Thus,

$$J_i(\tau)=\sum J_i(\tau,\,\lambda,\,\delta\lambda)\,,\quad \Delta\lambda_i=\sum\delta\lambda\,. \tag{11}$$

In this calculation, the spectral region between 1810 and 7300Å is divided into 122 wavelength intervals. This division of the spectrum is derived from ACKERMAN (1971) with the flux of solar photons at the top of the earth's atmosphere and the absorption cross-section of O_3 and O_2 at these intervals.

Computations are carried out for the ground albedo A=0.3 which is thought to be the global and time average value. The solar zenith angle χ is fixed at 45° throughout the computation.

2.2. *One-dimensional model*

The temporal variation in the number density of the ith constituent n_i is given by the following continuity equation if the vertical transport is parameterized through the eddy diffusion coefficient K_z.

$$\frac{\partial n_i}{\partial t}=P_i-L_in_i-K_z\left\{\frac{\partial n_i}{\partial z}+\left(\frac{1}{T}\frac{\partial T}{\partial z}+\frac{1}{H_{\mathrm{s}}}\right)n_i\right\}, \tag{12}$$

where T is the atmospheric temperature, and H_{s} the scale height of the mixed atmo-

sphere. P and $L_i n_i$ are the production and loss of n_i respectively.

A total of 38 chemical (and photochemical) reactions of O_x, NO_x and HO_x are included in the model. The atmospheric minor species calculated in the model are 11 species; $O_x(O(^3P)+O_3+O(^1D))$, $NO_x(N+NO+NO_2)$, HNO_3, $HO_x(H+HO+HO_2)$, and N_2O. $O(^1D)$, N, and H are assumed to be in a photochemical equilibrium. The vertical distribution of N_2, O_2, H_2, H_2O and CH_4 is fixed throughout the calculation.

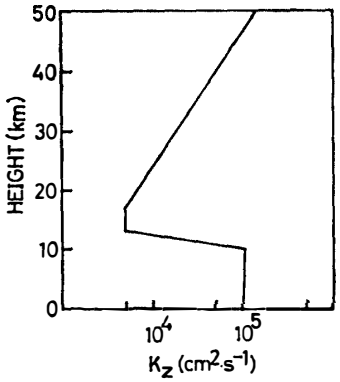

Fig. 1. Eddy diffusion coefficient profile.

Table 1. Chemical reactions in the model.

Reactions	Rate constant (cm^3 s^{-1}, cm^6 s^{-1})
$O(^1D)+M\rightarrow O+M$	1.8×10^{-11}
$O+O_2+M\rightarrow O_3+M$	$6.2\times10^{-34}(T/300)^{-2}$
$O_3+O\rightarrow 2O_2$	$1.5\times10^{-11}\exp(-2218/T)$
$O(^1D)+O_3\rightarrow 2O_2$	2.5×10^{-10}
$H+O_2+M\rightarrow HO_2+O_2$	$5.5\times10^{-32}(T/300)^{-1.4}$
$HO_2+O\rightarrow OH+O_2$	4.0×10^{-11}
$OH+O\rightarrow H+O_2$	$2.3\times10^{-11}\exp(110/T)$
$H+O_3\rightarrow OH+O_2$	$1.4\times10^{-10}\exp(-470/T)$
$OH+O_3\rightarrow HO_2+O_2$	$1.6\times10^{-12}\exp(-940/T)$
$HO_2+O_3\rightarrow OH+2O_2$	$1.1\times10^{-14}\exp(-580/T)$
$H_2O+O(^1D)\rightarrow 2OH$	2.2×10^{-10}
$H+HO_2\rightarrow H_2+O_2$	1.36×10^{-11}
$OH+HO_2\rightarrow H_2O+O_2$	4.0×10^{-11}
$H_2+O(^1D)\rightarrow H+OH$	9.9×10^{-11}
$N_2O+O(^1D)\rightarrow N_2+O_2$	1.1×10^{-10}
$\rightarrow 2NO$	6.6×10^{-11}
$NO+O_3\rightarrow NO_2+O_2$	$2.3\times10^{-12}\exp(-1450/T)$
$NO_2+O\rightarrow NO+O_2$	9.3×10^{-12}
$N+O_3\rightarrow NO+O_2$	1.0×10^{-15}
$N+NO\rightarrow N_2+O$	$5.1\times10^{-11}\exp(-170/T)$
$N+O_2\rightarrow NO+O$	$1.02\times10^{-14}T\exp(-3130/T)$
$OH+NO_2+M\rightarrow HNO_3+M$	$3.4\times10^{-30}/(1+8.4\times10^{-19}M)$
$HNO_3+OH\rightarrow H_2O+NO_3$	$1.5\times10^{-14}\exp(650/T)$
$HNO_3+O\rightarrow OH+NO_3$	1.0×10^{-14}
$HO_2+NO\rightarrow OH+NO_2$	$3.5\times10^{-12}\exp(250/T)$
$CH_4+OH\rightarrow CH_3+H_2O$	$2.35\times10^{-12}\exp(-1710/T)$
$CH_4+O(^1D)\rightarrow CH_3+OH$	1.4×10^{-10}

The eddy diffusion coefficient profile illustrated in Fig. 1, and chemical reactions in the model listed in Table 1 are quoted from MATSUNO and SHIMAZAKI (1981). The numerical technique used to solve eq. (12) is that described by SHIMAZAKI and OGAWA (1974). The boundary conditions are assumed to be fixed or time varying source-dependent concentrations at the surface and flux condition at the upper boundary of 50 km. The concentration of O_3 at the lower boundary is fixed.

2.3. Model atmosphere

The model atmosphere extended from the ground to 50 km, and was divided into 50 equally spaced intervals. Above the 50 km height, the atmosphere is regarded as a homogeneous layer of the scale height at an altitude of 50 km. The profiles of atmospheric temperature and molecular number density are taken from the model of the "U.S. Standard Atmosphere (U.S. Government Office, Washington, D.C., 227 p., 1976)". Initial values of ozone concentrations are also taken from that.

The various parameters for an aerosol model such as the refractive index, the size distribution and the height distribution are given as follows. The composition of the particles is taken to consist of impure sulphuric acid droplets at all heights. The real part of the refractive index as a function of wavelength is based on the experimental data of PALMER and WILLIAMS (1975) which correspond to the aerosol composition of 75% sulphuric acid in water solution (TOON and POLLACK, 1976), while the imaginary part which depends on the amount of impurities is assumed to be 0.005, independent of wavelength.

The size distribution function is assumed to follow the Zold distribution,

$$\frac{dN}{dr} = C \exp\left(-\frac{\ln^2(r/r_m)}{2\ln^2\sigma}\right) \quad \text{for} \quad 0.01 < r < 3.0\ \mu\text{m}\ , \tag{13}$$

where N and r are the number density and radius of particles respectively. C is a constant, and the standard deviation σ and the mode radius r_m of the distribution are taken to be 2 and 0.035 μm respectively (TOON and POLLACK, 1976).

To investigate the effects of the aerosol loads, the vertical distribution of aerosol is examined for 3 cases. a) Background case; that is based on the attenuation data of ELTERMAN (1968). b) Heavy stratospheric aerosol case; this distribution corre-

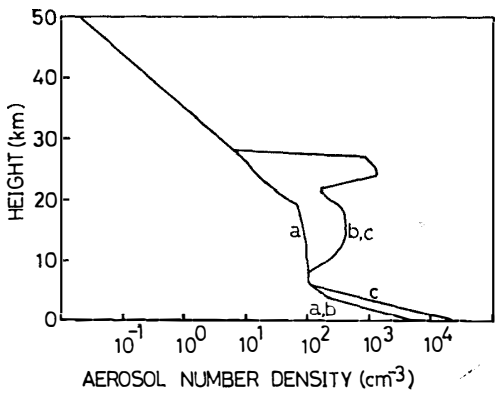

Fig. 2. Aerosol concentration profiles: (a) average concentration, (b) heavy aerosol concentration in the stratosphere, (c) heavy aerosol concentration at all heights.

sponds to the increase of aerosols after the eruptions of El Chichon observed by a Nd-YAG lidar at Fukuoka (HIRONO and SHIBATA, 1983). The scattering ratio of aerosol around 25 km on May 3, 1982 is in excess of 100 times greater than that of the background level. c) Heavy atmospheric aerosol at all heights; tropospheric aerosol load for a hazy condition is added to case b).

Figure 2 shows the vertical concentration profiles of aerosols used in the model. The equivalent number density in the figure is calculated from extinction profiles of aerosols by the Mie scattering theory using the refractive index and the size distribution given above.

3. Results

3.1. Photodissociation coefficients

Figure 3 shows the photodissociation coefficient profiles of molecular species with no aerosol load. This set of profiles supplies a reference for the case when aerosols are present.

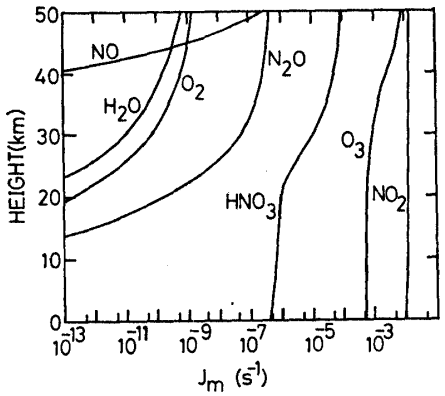

Fig. 3. Photodissociation coefficient profiles for the molecular atmosphere.

Figure 4 shows the changes in the photodissociation coefficients of some species for the aerosol cases a, b and c, compared to those in the case of a molecular atmosphere. For the background aerosol loads (case a), three different types of photodissociation changes are seen. For O_2, H_2O and N_2O molecules, their photodissociation rates change little above the aerosol layer and decrease dominantly below the aerosol layer. These molecules photodissociate in the wavelengths shorter than 2900Å which cannot penetrate into the troposphere due to the absorption of the stratospheric ozone layer. The photodissociation rates of O_3 and NO_2 increase at all altitudes except the boundary layer below 2 km. These molecules photodissociate even for wavelengths longer than 3200Å. These longer wavelengths are transmitted at all altitudes except the boundary layer. The radiation scattered by the aerosol layer enhances their photodissociation rates. HNO_3 molecules dissociate mainly between these two wavelength regions. Its photodissociation rates increase by a few percent in an altitude range of 15–25 km, and decrease below 15 km, in comparison with those for a molecular atmosphere. These three spectral regions for

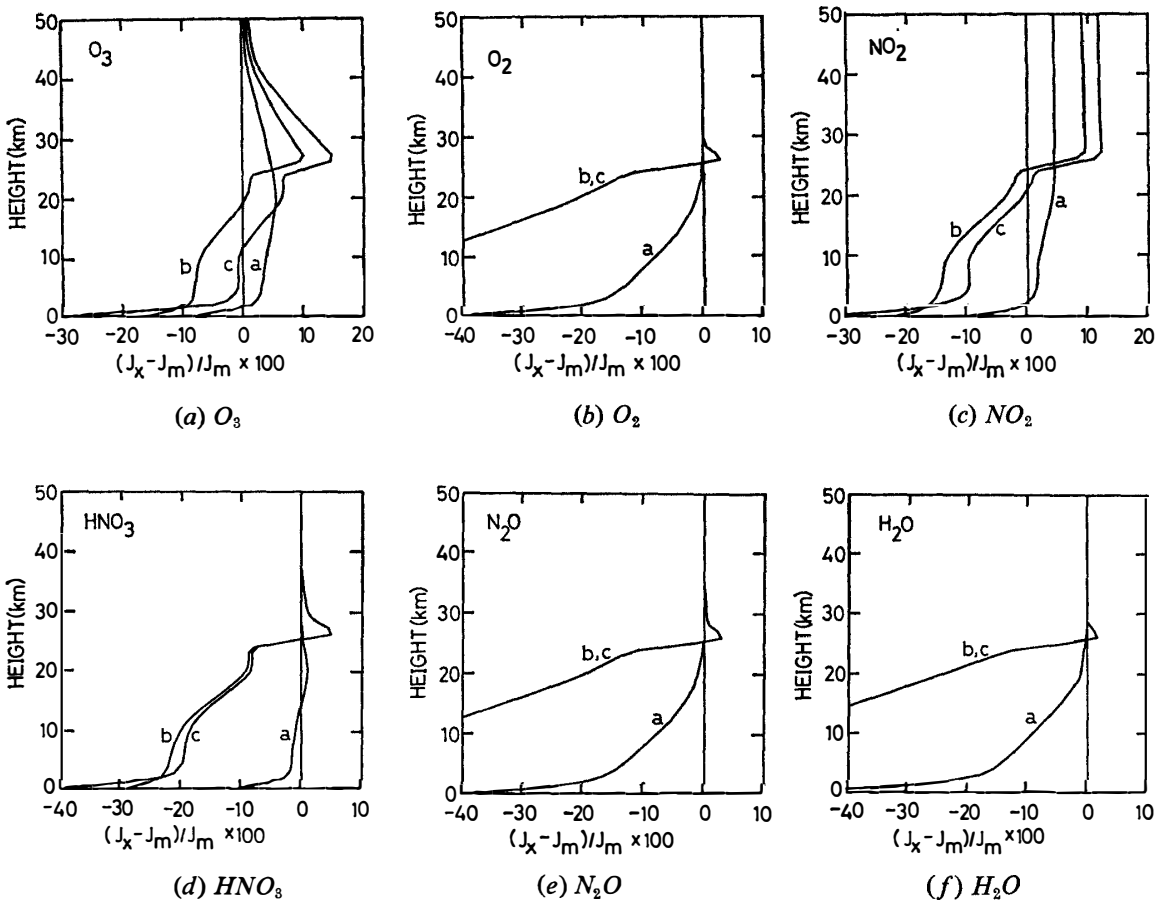

(*a*) O_3 (*b*) O_2 (*c*) NO_2

(*d*) HNO_3 (*e*) N_2O (*f*) H_2O

Fig. 4. Changes in the photodissociation coefficients of the various species for the different aerosol loads.

atmospheric species photodissociations were divided and discussed for molecular multiple scattering and surface albedo except aerosols by LUTHER and GELINAS (1976).

For heavy aerosol loads such as the cases b and c, the changes of photodissociation rates of O_2, H_2O and N_2O show also similar profiles. Just above the intense aerosol layer due to El Chichon, their photodissociation rates increase by a few percent in comparison with the case a, and below the aerosol layer decrease due to extinction by aerosols. The differences of their photodissociations for the cases b and c are not recognized. For HNO_3, the photodissociation rates increase also just above 25 km, and decrease below 25 km.

The photodissociation rates of O_3 and NO_2 in the stratosphere are enhanced by the increase in the aerosol loads in comparison with the case a. For the case c, their photodissociation rates increase by about 12–15% at the 27 km altitude which is just above the aerosol layer by El Chichon. Compared with the background aerosol loads (case a), their photodissociation rates increase by about 10%. Below the intense stratospheric aerosol layer, their photodissociation rates decrease. Compared with the case a, the decrease for the case b is about 10–20%, and is larger than that for the case c. In the case of c, the diffuse fields by the hazy troposphere compensate the decrease.

The profile of the changes in the photodissociation rates of O_3 and the magnitudes of the increase for the case a is almost similar to those calculated by FIOCCO *et al.* (1978). A little difference below 10 km is due to that of tropospheric aerosol component. The dust particles are not included in our model. According to their results simulated for aerosol loads such as those obtained after the Mt. Agung 1963 eruption, the photodissociation rates of O_3 increase except the boundary layer. In the present simulation for the case b, the photodissociation rates decrease below about 18 km. This is because the amounts of aerosols by El Chichon are much larger than those by Mt. Agung. Effects of extinction by the stratospheric aerosols are larger than those of diffuse fields by the tropospheric aerosols.

3.2. Minor species concentrations

Figure 5 shows the concentration profiles for O_X, HO_X and NO_X species calculated by a one-dimensional model in the case of a molecular atmosphere (no aerosols). In order to investigate the effect of the aerosol loads, the concentration profiles calculated for the aerosol atmosphere are compared with these profiles.

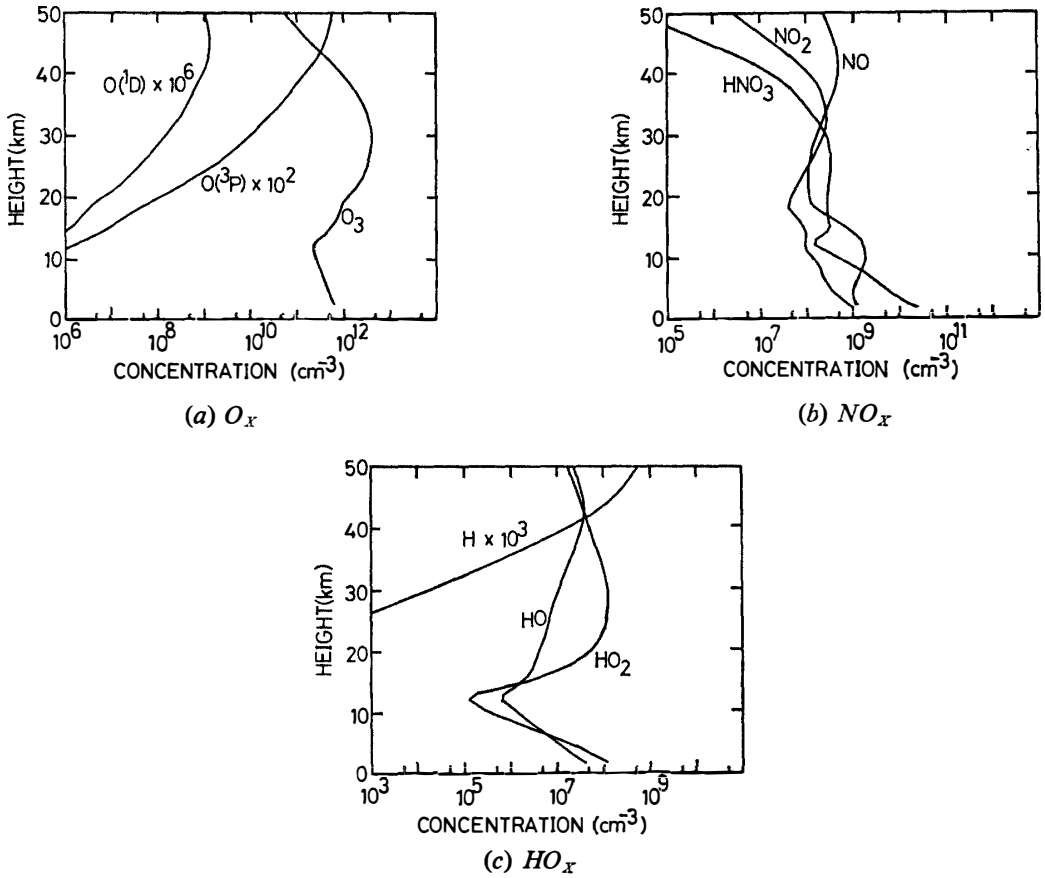

Fig. 5. Concentration profiles of O_X, NO_X and HO_X for the molecular atmosphere.

The percent deviations of the species concentrations calculated for the average aerosol load (case a) with respect to those for a molecular atmosphere are shown in Fig. 6. Figure 6a shows the changes in the concentration of O_X species due to the effect of aerosols in the case of a. The ozone concentration in the stratosphere de-

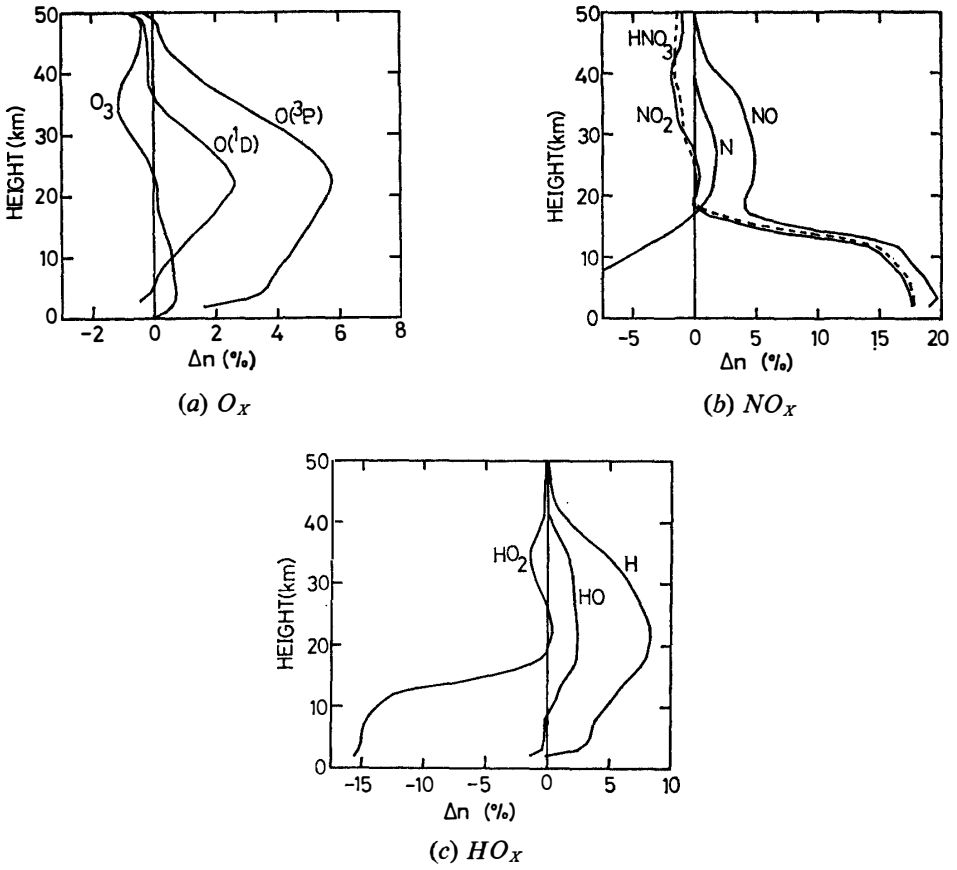

(a) O_X (b) NO_X (c) HO_X

Fig. 6. Changes in the concentration of O_X, NO_X and HO_X for the average aerosol load.

creases nearly one percent. This decrease is due to the enhancement of photodissociation of ozone. The increase in the concentration of $O(^1D)$ and $O(^3P)$ at all heights is obtained.

Figure 6b shows the changes in the concentrations of NO_X species. A small decrease in the concentration of NO_2 is obtained in the region of 20–40 km height due to the enhanced photodissociation rates of NO_2. A few percent increase of NO concentration in the 20–40 km region is due to the enhancement of photodissociation of NO_2.

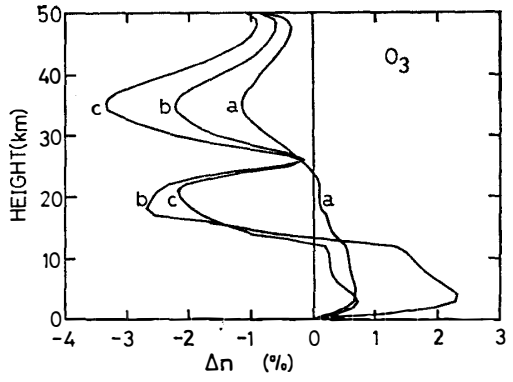

Fig. 7. Changes in the concentration of O_3 for the different aerosol loads.

Figure 6c shows the changes in the concentrations of HO_x species. Concentration of H increases by several percent at all heights except near the ground. A few percent increase in HO concentration in the 10–40 km region is obtained. This increase is due to the enhancement of photodissociation of HNO_3 and the increase in $O(^1D)$ concentration.

Figure 7 shows the changes in ozone concentration for different aerosol loads compared to that of a molecular atmosphere. In the stratosphere except at the 25 km height, increase in the aerosol loads leads to decrease in the ozone concentration. Ozone concentration decreases by about 4% in the 35 km region for heavy aerosol loads, and by 2% compared with the average aerosol loads (case a). At a height of 25 km, there is a dip in the changes in the concentration of O_3 for heavy aerosol loads. In the troposphere ozone concentration increases for any aerosol loads.

As it is difficult to explain qualitatively these characteristics of the changes in the ozone concentration for an oxygen-nitrogen-hydrogen atmosphere, we consider first of all a pure oxygen atmosphere. For changes of photodissociation coefficients of oxygen J_1 and ozone J_2, the change in ozone concentration $\Delta[O_3]$ is expressed as follows:

$$\Delta[O_3]/[O_3]_{eq}=\frac{1}{2}(\Delta J_1/J_1-\Delta J_2/J_2)\,.$$

For aerosol loads of case a, $\Delta J_1/J_1 \leqq 0$ and $\Delta J_2/J_2>0$ as shown in Fig. 4 and so ozone decreases at all heights. The decrease in ozone concentration was simulated in our model for a pure oxygen atmosphere for three cases of aerosol loads since the quantity in the parenthesis is negative as shown in Fig. 4. For an oxygen-nitrogen-hydrogen atmosphere, ozone increases below 20 km for the case a. The most probable constituent is like HO_2 for the ozone increase. The decrease of HO_2 increases O_3 since HO_2 is a most important species in controlling the amounts of ozone in the troposphere. The dip at a height of 20 km is due to the increase in J_1. However, it is difficult to explain the ozone increase, clearly, but for the decrease of total ozone, this increase is small by one order of magnitude compared with the decrease in the lower stratosphere since the maximum ozone concentration is around a height of 25 km.

4. Conclusion

The effects of radiation scattered by aerosols on the minor atmospheric species concentrations are examined by a one-dimensional transport-kinetics model coupled with the radiative transfer model. Aerosol increase in the stratosphere affects the photodissociation and changes the concentration profiles of minor constituents. As for ozone, the concentration decreases by a few percent in the stratosphere for the heavy aerosol load.

Changes in ozone concentration affect the temperature profile through changes in the heating (cooling) rate of atmosphere. Changes in the temperature affect the chemical reaction rates and in turn affect the composition. The temperature feedback mechanism must be considered.

Acknowledgments

The authors would like to express our gratitude to T. SHIBATA for valuable disscussion.

References

ACKERMAN, M. (1971): Ultraviolet solar radiation related to mesospheric processes. Mesospheric Models and Related Experiments, ed. by G. FIOCCO. Dordrecht, D. Reidel, 149–159.

DEIRMENDJIAN, M. (1969): Electromagnetic Scattering on Spherical Polydispersions. New York, Elsevier, 290 p.

ELTERMAN, L. (1968): UV, visible and IR attenuation for altitude to 50 km. AFCRL Rep., 68–0153.

FIOCCO, G., MUGNAI, A. and FORLIZZI, W. (1978): Effects of radiation scattered by aerosols on the photodissociation of ozone. J. Atmos. Terr. Phys., **40**, 949–961.

GRANT, I. P. and HUNT, G. E. (1969): Discrete space theory of radiative transfer. Proc. R. Soc. London, Ser. A, **313**, 183–197.

HIRONO, M. and SHIBATA, T. (1983): Enormous increase of stratospheric aerosol over Fukuoka due to volcanic eruption of El Chichon in 1982. Geophys. Res. Lett., **10**, 152–154.

LUTHER, F. M. and GELINAS, R. J. (1976): Effect of molecular multiple scattering and surface albedo on atmospheric photodissociation rates. J. Geophys. Res., **81**, 1125–1132.

LUTHER, F. M., WUEBBLES, D. J., DUEWER, W. H. and CHANG, J. S. (1978): Effect of multiple scattering on species concentrations and model sensitivity. J. Geophys. Res., **83C**, 3563–3570.

MATSUNO, T. and SHIMAZAKI, T. (1981): Seisôken to Chûkanken no Taiki (Stratospheric and Mesospheric Atmosphere). Tokyo, Tokyo Univ. Press, 279 p. (Taiki Kagaku Kôza 3).

MEADOR, W. E. and WEAVER, W. R., (1980): Two-stream approximations to radiative transfer in planetary atmospheres; A unified description of existing methods and a new improvement. J. Atmos. Sci., **37**, 630–643.

MUGNAI, A., PETRONCELLI, P. and FIOCCO, G. (1979): Sensitivity of the photodissociation of NO_2, NO_3, HNO_3, and H_2O_2 to the solar radiation diffused by the ground and by atmospheric particles. J. Atmos. Terr. Phys., **41**, 351–359.

PALMER, K. F. and WILLIAMS, D. (1975): Optical constants of sulfuric acid; application to the clouds of Venus? Appl. Opt., **14**, 208–219.

PENNDOLF, R. (1957): Tables of the refractive index for standard air and Rayleigh scattering coefficient for the spectral region between 0.2 and 20.0 μ and their application to atmospheric optics. J. Opt. Soc. Am., **47**, 176–182.

PITARI, G. and VISCONTI, G. (1979): A simple method to account for Rayleigh scattering effects on photodissociation rates. J. Atmos. Sci., **36**, 1803–1811.

SHIMAZAKI, T. and OGAWA, T. (1974): On the theoretical model of vertical distributions of minor neutral constituents in the stratosphere. Tech. Memo. ERL OD-20, Boulder, NOAA.

TOON, O. B. and POLLACK, J. B. (1976): A global average model of atmospheric aerosols for radiative transfer calculations. J. Appl. Meteorol., **15**, 225–246.

WISCOMBE, W. J. (1976a): Extention of the doubling method to inhomogeneous sources. J. Quant. Spectrosc. Radiat. Transfer, **16**, 477–489.

WISCOMBE, W. J. (1976b): On initialization; error and flux conservation in the doubling method. J. Quant. Spectrosc. Radiat. Transfer, **16**, 637–658.

(Received March 31, 1983; Revised manuscript received June 13, 1983)